Trapped-Particle Asymmetry Modes in Single-Species Plasmas

A. A. Kabantsev, C. F. Driscoll, T. J. Hilsabeck, T. M. O'Neil, and J. H. Yu
Physics Department, University of California, San Diego, California 92093-0319
(Received 5 September 2001; published 9 November 2001)

Novel trapped-particle asymmetry modes propagate on cylindrical electron columns when axial variations in the wall voltage cause particle trapping. These modes consist of $\mathbf{E} \times \mathbf{B}$ drifts of edge-trapped particles, partially shielded by axial flows of interior untrapped particles. A simple model agrees well with the observed frequencies and eigenfunctions, but the strong mode damping is as yet unexplained. These modes may be important in coupling trap asymmetries to particle motions and low frequency $\mathbf{E} \times \mathbf{B}$ drift modes.

DOI: 10.1103/PhysRevLett.87.225002 PACS numbers: 52.27.Jt, 52.25.Fi, 52.35.–g

Single-species plasmas confined in cylindrical traps with static electric and magnetic fields are utilized in research ranging from basic plasma and fluid dynamics to spectroscopic frequency standards to antimatter containment [1]. The plasma confinement times can be hours or days, generally limited by azimuthal asymmetries in the trapping fields, which couple angular momentum into the rotating plasma [2]. This coupling can be enhanced by mode resonances [3], and plasma modes occur on frequency scales ranging from the (high) cyclotron frequency Ω_c, to the plasma frequency ω_p, to the (low) $\mathbf{E} \times \mathbf{B}$ drift frequency ω_E. However, the well-studied "diocotron" drift modes have axial wave number $k_z \simeq 0$, and so do not readily couple the plasma electrostatic energy into particle kinetic energy.

Here, we describe novel "trapped-particle asymmetry" modes that propagate azimuthally at low $\mathbf{E} \times \mathbf{B}$ drift frequencies but that have $k_z \neq 0$ and thus couple to particle kinetics. These modes exist when axial variations in the wall potential cause the equilibrium plasma to have axially trapped particles. Experimentally, we generate the trapped particles by applying a "squeeze" voltage to a central cylindrical electrode, but smaller trapping potentials are caused by wall irregularities and are probably endemic to these traps.

These asymmetry modes can have an azimuthal mode number $m = 1, 2, \ldots,$ but we focus on $m = 1$ here. Dynamically, the modes are an $\mathbf{E} \times \mathbf{B}$ drift motion of the edge-trapped particles with axial flows of interior untrapped particles giving partial Debye shielding. A simple theory model with these characteristics shows close correspondence with the measured frequencies and radial eigenfunctions of the modes. Experimentally, the modes are observed to be exponentially damped, but this damping is not yet understood. These modes are particularly simple cylindrical analogs to the trapped drift modes which can contribute to anomalous plasma transport in tokamak-like and toroidal multipole configurations of neutral plasmas [4,5].

The cylindrical confinement geometry and a schematic of the mode are shown in Fig. 1. A nominally cylindrical column of electrons emitted from a hot tungsten source is confined radially by a uniform magnetic field $B = 4$ kG and confined axially by negative voltages $-V_c = -100$ V on end cylinders. Typical electron columns have a central density $n_0 \approx 1.5 \times 10^7\ \mathrm{cm}^{-3}$ over a length $L_p \approx 50$ cm, with a column radius of $R_p \approx 1.2$ cm inside a wall radius $R_w = 3.5$ cm. The z-averaged electron density $n(r, \theta, t)$ can be (destructively) measured at any time by dumping the electrons axially onto a phosphor screen imaged by a CCD camera [6].

The individual electrons have a thermal energy $T \approx 1$ eV, giving an axial bounce frequency $f_b \equiv \bar{v}/2L_p \approx 0.5$ MHz and a Debye shielding length $\lambda_D \equiv (T/4\pi e^2 n)^{1/2} \approx 0.2$ cm. The unneutralized electron charge results in a central potential $-\phi_0 \approx -30$ V, and the radial electric field causes the column to $\mathbf{E} \times \mathbf{B}$ drift rotate at a rate $f_E(r) \equiv cE(r)/2\pi rB \lesssim 50$ kHz. Figure 2 shows typical radial profiles of density and rotation for the quiescent, θ-symmetric, quasi-steady-state columns on which we study the waves.

When a negative squeeze voltage $-V_{\mathrm{sq}}$ is applied to a central cylinder, electrons are excluded from the column periphery under the squeeze ring, and those electrons located at radii at $r > r_s$ are trapped axially in one end or the other. For small V_{sq}, a fraction $\varepsilon_{\mathrm{tr}} \approx V_{\mathrm{sq}}/\phi_0$ of all the electrons are trapped axially.

Linear $\mathbf{E} \times \mathbf{B}$ drift modes with azimuthal mode numbers $m = 1, 2, \ldots$ propagate on this trapped-particle equilibrium. The ubiquitous $m = 1$ center-of-mass diocotron

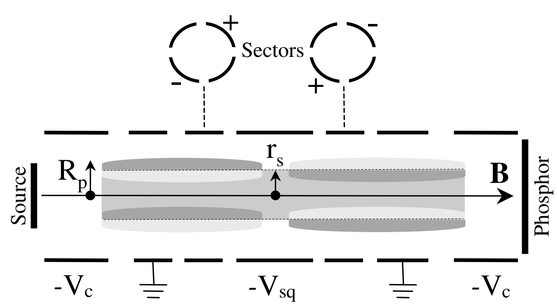

FIG. 1. Schematic of the cylindrical trap and squeezed electron column with asymmetry mode, showing the positive and negative trapped and untrapped density perturbations.

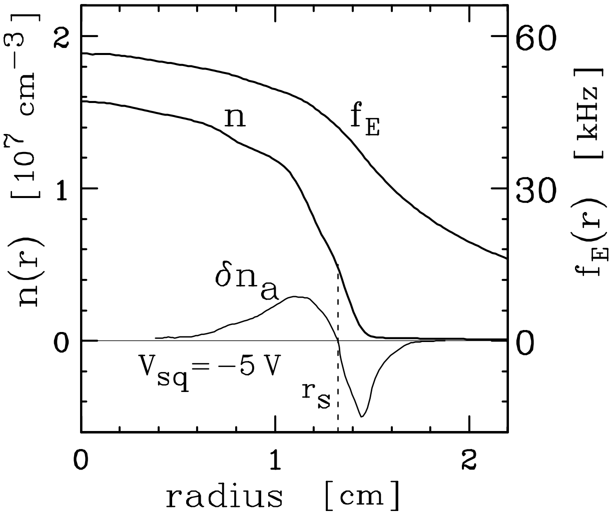

FIG. 2. Radial profiles of density $n(r)$, $\mathbf{E} \times \mathbf{B}$ rotation frequency $f_E(r)$, and measured asymmetry mode eigenfunction $\delta n_a(r)$.

mode is essentially uniform in z (i.e., $k_z \approx 0$) and is nominally unaffected by small $V_{\rm sq}$. In contrast, the $m = 1$ trapped-particle asymmetry mode described here has odd parity in z: the perturbations are essentially uniform within each end but of *opposite sign* on either side of the squeeze, as shown schematically in Fig. 1. Moreover, the perturbations in the trapped particles at $r > r_s$ are partially "shielded" by perturbations of opposite sign in the untrapped particles at $r < r_s$, and these untrapped particles slosh from end to end in response to the $\mathbf{E} \times \mathbf{B}$ drift evolution of the trapped particles.

Experimentally, these odd-z-parity $m = 1$ asymmetry modes are excited with a short burst of 1–10 sinusoidal oscillations which are phased $+$ and $-$ on θ-opposite and z-opposite wall sectors, as shown in Fig. 1. The asymmetry mode could actually be excited from any single sector, but the configuration above minimizes the concurrent excitation of other modes. Any single wall sector can be used as a receiver, or sectors can be used in combination to verify the θ and z symmetries of the modes.

Figure 3 shows the measured frequencies f_a and damping rates γ_a for the trapped-particle asymmetry mode as the applied squeeze voltage $V_{\rm sq}$ is varied. The frequency f_d of the diocotron mode is also shown for reference. The asymmetry mode frequency is at or near the edge rotation frequency $f_E(R_p)$ for $V_{\rm sq} \ll \phi_0$. As $V_{\rm sq}$ is increased, the trapping separatrix r_s moves inward, and f_a decreases. For $V_{\rm sq} \gtrsim \phi_0$, the column is cut in half, and the asymmetry mode becomes degenerate with the diocotron mode. With all particles trapped, the asymmetry mode is equivalent to two separate diocotron modes, 180° out of phase. The diocotron frequency f_d increases slightly with $V_{\rm sq}$, because the effective line density of the column increases as particles are excluded from the squeeze ring. Both f_a and f_d scale as $f \propto B^{-1}$, as expected for $\mathbf{E} \times \mathbf{B}$ drift modes.

The asymmetry mode is observed to damp exponentially with time; that is, the received wall signals are basically

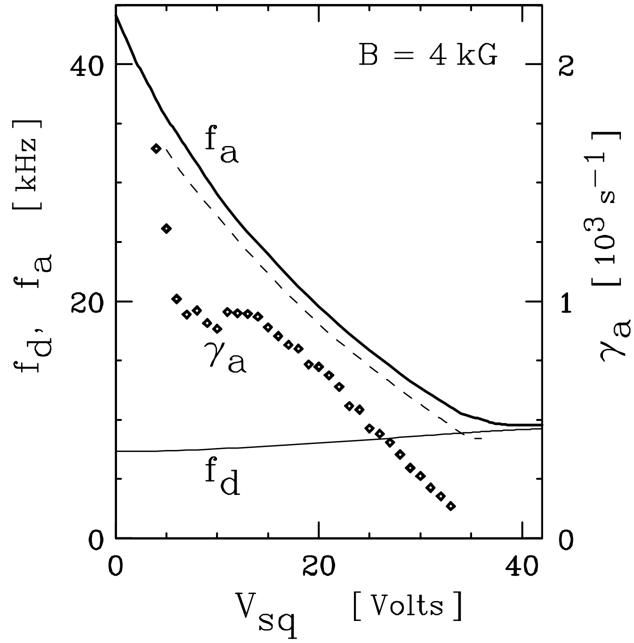

FIG. 3. Measured frequencies f_a and f_d and decay rate γ_a vs squeeze voltage $V_{\rm sq}$, and f_a calculated from the kinetic model (dashed line).

sinusoidal, decreasing in amplitude as $\exp(-\gamma_a t)$. The damping rate γ_a depends on $V_{\rm sq}$ decreasing roughly as $(f_a - f_d)$ in the regime $V_{\rm sq} \gtrsim \phi_0/10$ where γ_a can be readily measured. Figure 3 shows that $\gamma_a/f_a \lesssim 1/20$, so the mode is strongly damped except at $V_{\rm sq} \gtrsim \phi_0$. However, we observe essentially no magnetic field dependence to the damping in the range of 0.5 kG $\leq B \leq$ 10 kG, i.e., $\gamma_a \propto B^0$. Thus, $\gamma_a/f_a \propto B^1$ and the mode is relatively less strongly damped at lower magnetic fields.

As yet, the cause of this damping is not understood, but experimental signatures suggest diffusive mixing between the trapped and untrapped populations. Also, for $V_{\rm sq} < \phi_0/10$, there are suggestions that spatial Landau damping (scaling as B^{-1}) may occur, but this damping depends critically on the density profile near R_p.

The density eigenfunctions $\delta n_a(r)$ of the asymmetry mode can be obtained from a time sequence of measurements of the density $n_h(r, \theta, t)$ z averaged over only *half* the plasma. Here, time $t = 0$ is defined by the wave excitation, so the measured n_h is synchronous with the wave. The density perturbations associated with each mode are essentially independent of z over each half of the plasma, but the asymmetry mode perturbation changes sign at the squeeze barrier. To dump only half the column onto the phosphor screen, $V_{\rm sq}$ is increased to 100 V immediately before lowering V_c.

The $m = 1$ perturbations in $n_h(r, \theta, t)$ are then fit to a sum of two modes (asymmetry and diocotron), as

$$\int d\theta \, n_h(r, \theta, t) e^{-im\theta} = \sum_{j=a,d} \delta n_j(r) e^{i2\pi f_j t - \gamma_j t}.$$

The residual to this fit is small, so the eigenfunctions are obtained with little ambiguity, and the f_j and γ_j match the wall sector time sequence data. The real part of the asymmetry mode eigenfunction δn_a (scaled arbitrarily) obtained for $V_{\mathrm{sq}} = 5$ V is shown below $n(r)$ in Fig. 2; with proper choice of θ origin, the imaginary part of δn_a is essentially zero.

The mode shows a negative perturbation at $r > r_s$ and a positive perturbation for $r < r_s$, and the signs of these perturbations reverse for $z \rightarrow -z$ and for $\theta \rightarrow \theta + \pi$. The observed position of the zero crossing at r_s varies with V_{sq}, consistent with the "waistline" radius obtained from (r, z) Poisson solutions for the equilibrium with the measured charge and applied wall potentials.

Fluid theory and kinetic theory models further support the interpretation of the asymmetry mode as trapped $\mathbf{E} \times \mathbf{B}$ drifting edge particles which are Debye shielded by sloshing interior particles. In these models, the applied squeeze voltage is presumed to create a (zero-length) barrier for particles at $r > r_s$, creating two outer regions with axial lengths L_1 and L_2. In contrast, interior particles with $r < r_s$ move freely over length $L_1 + L_2$.

Because the axial bounce frequency is large compared to the $\mathbf{E} \times \mathbf{B}$ rotation frequency and the mode frequency, the bounce-average density perturbation in any one of the three regions, $\overline{\delta n}$, is related to the bounce-average potential perturbation in that region, $\overline{\delta \phi}$, through

$$\overline{\delta n}(r) = \frac{c}{2\pi B r} \frac{\partial n_0}{\partial r} \frac{m \overline{\delta \phi}(r)}{m f_E(r) - f}. \tag{1}$$

Within any of the regions, rapid axial streaming yields the adiabatic response

$$\delta n(r,z) = \overline{\delta n}(r) + \frac{e n_0}{T} [\delta \phi(r,z) - \overline{\delta \phi}(r)]. \tag{2}$$

This type of response gives rise to Debye shielding, making $\delta \phi(r,z)$ and $\delta n(r,z)$ nearly z independent except near the plasma ends and the squeeze region. Thus, we approximate $\delta n(r,z) \approx \delta n_j(r)$ and $\delta \phi(r,z) \approx \delta \phi_j(r)$, with $j = 1, 2$ representing the left and right sides relative to the barrier. Poisson's equation for the two sides is then

$$\frac{1}{r} \frac{\partial}{\partial r} r \left(\frac{\partial}{\partial r} \delta \phi_j \right) - \frac{m^2}{r^2} \delta \phi_j = \begin{cases} \dfrac{2ec}{Br} \dfrac{\partial n_0}{\partial r} \dfrac{m \delta \phi_j}{m f_E - f}, & r > r_s, \\ \dfrac{2ec}{Br} \dfrac{\partial n_0}{\partial r} \dfrac{m \delta \phi_b}{m f_E - f} + \dfrac{4\pi e^2 n}{T} (\delta \phi_j - \delta \phi_b), & r < r_s. \end{cases} \tag{3}$$

Here, $\delta \phi_b \equiv (L_1 \delta \phi_1 + L_2 \delta \phi_2)/(L_1 + L_2)$ is the potential averaged over both sides, and the boundary condition is $\delta \phi_j(R_w) = 0$.

Fortunately, the even and odd axial symmetries of the diocotron and asymmetry modes decouple the equations. For $\delta \phi_1(r) = \delta \phi_2(r) = \delta \phi_b(r)$, both equations reduce to the usual equation for a diocotron mode. For $L_1 \delta \phi_1(r) = -L_2 \delta \phi_2(r)$, giving $\delta \phi_b(r) = 0$, we obtain an eigenvalue equation for the asymmetry mode potentials.

For a uniform density profile of density n_0 and radius R_p, the eigenfrequency $f \equiv f_a$ is

$$\frac{f_a}{f_E(0)} = m - \frac{(R_w^{2m} - R_p^{2m})(I_{m-1} R_p^{2m} - I_{m+1} r_s^{2m})}{R_p^{2m}(I_{m-1} R_w^{2m} - I_{m+1} r_s^{2m})}. \tag{4}$$

Here, $I_{m\pm1} \equiv I_{m\pm1}(r_s/\lambda_D)$ are modified Bessel functions of the first kind. In the limit of $\lambda_D \rightarrow 0$, the interior region acts like a conductor, and the exponentially large $I_{m\pm1}$ may be replaced by 1 in Eq. (4).

The boundary r_s is determined by radial integration of Poisson's equation: integration of density n_0 out to radius r_s gives $\phi(R_w) = -V_{\mathrm{sq}}$. Figure 4 shows r_s, f_a, and f_d versus V_{sq} for this uniform density model with $R_p = 0.5 R_w$ and $m = 1$. There is an obvious general correspondence between this coarse estimate and the experiment (Fig. 3).

A kinetic analysis allowing for trapped and untrapped particles coexisting at each radius gives a more realistic approximation to the experiments. The squeeze causes a potential barrier of strength $\Delta\phi(r)$, giving a trapped-particle density $n_t(r) = n(r)\,\mathrm{erf}[(e\Delta\phi/T)^{1/2}]$ and an untrapped density $n_u = n - n_t$. The equilibrium Poisson solutions show that $\Delta\phi$ is essentially zero for small radii and that it rises sharply near r_s to a value much larger than T. Thus, the kinetic treatment essentially smooths the discrete transition model over a radial scale of a few λ_D.

The frequency f_a versus V_{sq} predicted by this kinetic theory using the measured $n(r)$ and the calculated $\Delta\phi(r)$ is given by the dashed curve in Fig. 3, showing close agreement with the measured frequencies. The 10% discrepancy

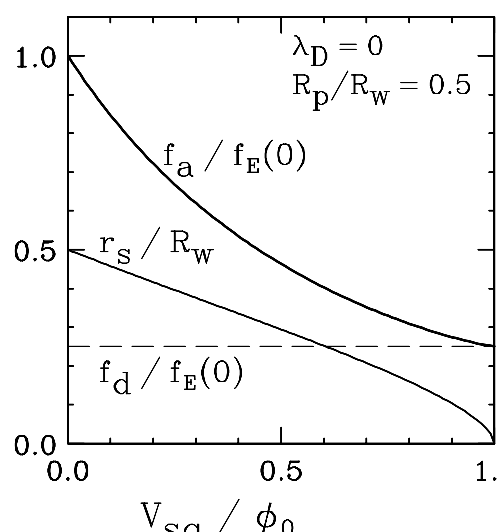

FIG. 4. Separatrix radius r_s vs V_{sq}/ϕ_0 for the uniform density model, giving f_a from Eq. (4) and constant f_d.

may reflect the nonzero length of the barrier and consequent increase in trapped-particle densities.

Similarly, the eigenfunctions $\delta n_a(r)$ obtained from the kinetic analysis show general correspondence with experiments, although the measured eigenfunctions in the untrapped region of $r < r_s$ are smaller than predicted by a factor of approximately r_s/R_p. This discrepancy may reflect systematic errors in the dump imaging, or it may be related to particle diffusion and decay of the mode.

Although the asymmetry modes can propagate in a trap with perfect θ symmetry, our larger interest is in traps with (inevitable) θ asymmetries. These asymmetries commonly arise from construction imperfections in the trap walls (especially the sectored cylinders) or in the magnet. The asymmetries can have arbitrary θ and z dependence, but it is common to refer to their dominant m and k_z components. One of the more prevalent asymmetries is a $m = 1$, $k_z = \pi/L_p$ "tilt" of the magnetic field with respect to the trap axis, characterized by an angle $\theta_B \equiv B_\perp/B_z$.

The qualitative behavior of the asymmetry mode remains unchanged even with moderately large magnetic tilt. Figure 5 shows f_a decreasing by 30% and γ_a decreasing by 60% at fixed $V_{sq} = -10$ V as the magnetic tilt is increased to $\theta_B = \pm 3 \times 10^{-3}$ rad. These quantitative changes are mainly due to a decrease in the plasma potential ϕ_0 (caused by tilt-induced particle transport), causing the ratio V_{sq}/ϕ_0 to increase and the effective trapping barrier to be enhanced.

Trapped particles may be an inherent part of Penning-Malmberg traps for a variety of reasons. Some intentional manipulations, such as "squeeze damping" of the diocotron mode [7,8] obviously create equilibria as described here. The wide variety of "nested traps" being built for overlapping confinement of positrons and antiprotons [9,10] have populations of trapped and untrapped particles. Most subtly, z variations in the effective wall voltage can arise from small unintentional construction anomalies. For example, a variation in wall radius among cylinders gives an effective potential $V_{sq} \approx \phi_0 \Delta R_w/R_w$; this gives a trapped fraction $\varepsilon_{tr} \approx \Delta R_w/R_w$, so $\varepsilon_{tr} \gtrsim 10^{-3}$ is probably common to all devices.

The existence of trapped-particle asymmetry modes substantially alters the theory perspective on particle transport due to θ asymmetries in the trap construction. Resonant particle transport theories [3] utilize integration along unperturbed orbits, which is invalid with the bulk trapped-particle populations described here, or even with microscopic trapping [11]. Similarly, 2D bounce-averaged invariants suggest that particles are confined to equipotential surfaces, and a k_z variation is required for radial particle transport; however, all previously known modes with $k_z \neq 0$ have frequencies near ω_p as opposed to f_d.

Experimentally, there are strong suggestions that the asymmetry mode contributes to asymmetry-induced transport by coupling between the $k_z \neq 0$ asymmetry and the $k_z \approx 0$ diocotron mode. For the case of a magnetic tilt θ_B, the diocotron mode has axially sloshing particles [12] at frequency f_d but remains essentially undamped. However, coupling to the axially sloshing particles in the strongly damped asymmetry mode may result in diocotron mode damping and bulk radial transport of particles. The characteristics of this coupling are presently being investigated.

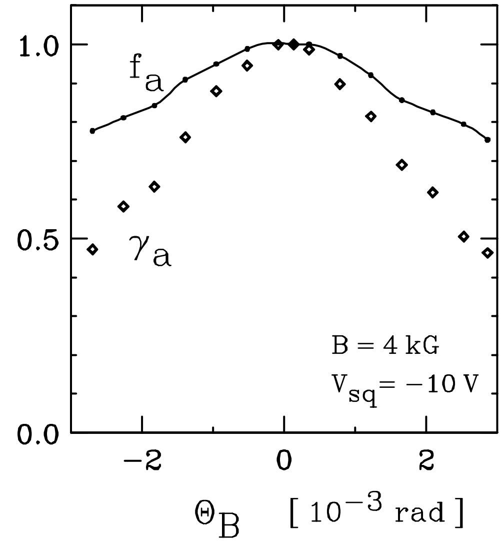

FIG. 5. Measured frequency f_a and decay rate γ_a vs magnetic tilt θ_B, normalized to values at $\theta_B = 0$.

This work is supported by Office of Naval Research Grant No. ONR N00014-96-1-0239 and National Science Foundation Grant No. PHY-9876999.

[1] *Non-Neutral Plasma Physics III,* edited by J. J. Bollinger, R. L. Spencer, and R. C. Davidson, AIP Conf. Proc. No. 498 (AIP, Melville, NY, 1999).
[2] J. M. Kriesel and C. F. Driscoll, Phys. Rev. Lett. **85**, 2510 (2000).
[3] D. L. Eggleston and T. M. O'Neil, Phys. Plasmas **6**, 2699 (1999).
[4] A. J. Redd *et al.,* Phys. Plasmas **6**, 1162 (1999).
[5] M. Nadeem *et al.,* Plasma Phys. Controlled Fusion **37**, 1169 (1995).
[6] K. S. Fine, W. G. Flynn, A. C. Cass, and C. F. Driscoll, Phys. Rev. Lett. **75**, 3277 (1995).
[7] B. P. Cluggish, Ph.D. thesis, University of California at San Diego, 1995.
[8] K. S. Fine, Ph.D. thesis, University of California at San Diego, 1989.
[9] M. Charlton *et al.,* Phys. Rep. **214**, 67 (1994).
[10] D. Hall and G. Gabrielse, Phys. Rev. Lett. **77**, 1962 (1996).
[11] D. H. E. Dubin, Phys. Rev. Lett. **79**, 2678 (1997).
[12] G. W. Hart, Phys. Fluids B **3**, 2987 (1991).